Title	Simultaneous measurements of LII/LIF/LIS on single-coal-particle combustion
Author(s)	Sawada, Shinya; Okada, Daisuke; Tainaka, Kazuki et al.
Citation	Applied Physics B. 2023, 129, p. 159
Version Type	AM
URL	https://hdl.handle.net/11094/92586
rights	
Note	

Simultaneous Measurements of LII/LIF/LIS on Single-Coal-Particle Combustion

Shinya Sawada[1*], Daisuke Okada[1], Kazuki Tainaka[2], Noriaki Nakatsuka[1], Tsukasa Hori[1], Jun Hayashi[3] and Fumiteru Akamatsu[1]

[1*]Mechanical Engineering, Osaka University, 2-1, Yamadaoka, Suita, 5650871, Osaka, Japan.

[2]Energy Transformation Research Laboratory, Central Research Institute of Electric Power Industry (CRIEPI), 2-6-1, Nagasaka, Yokosuka, 2400196, Kanagawa, Japan.

[3]Energy Conversion Science, Kyoto University, Yoshida-honmachi, Sakyo-ku, 6068501, Kyoto, Japan.

*Corresponding author(s). E-mail(s): ssawada@mech.eng.osaka-u.ac.jp;

Abstract

Simultaneous imaging of polycyclic aromatic hydrocarbons (PAHs), soot, and the flame zone formed around a single coal particle was conducted to investigate the flame structure of a single coal particle. The spatial distribution of PAHs, soot, and the flame zone were illuminated using PAHs and CH_2O laser-induced fluorescence (LIF) and laser-induced incandescence (LII), respectively. Additionally, the spatial distribution of the primary soot particle size was evaluated using a combination of LII and laser-induced scattering (LIS). The results showed that the CH_2O-LIF imaging was successful for the volatile flame of a single pulverized coal particle. The PAHs-LIF signal was found inside the region where the LII signal was measured, while the CH_2O-LIF signal was detected outside of the LII signal. The size of soot particles increased, and the soot number density decreased from the interior to the exterior of the volatile flame. Furthermore, the structure of the volatile flame of a single coal particle was found to be identical to that of a diffusion flame.

Keywords: Coal particle, Laser Induced Incandescence, Laser Induced Fluorescence of PAHs and CH_2O, Laser Induced Scattering

1 Introduction

Coal is a vital energy resource in electricity production, because of its affordability and reliable supply[1]. Given that most heat transfer in boilers occurs through radiation, it is essential to comprehend the formation of soot, which acts as a radiation carrier[2]. A comprehensive understanding of radiation facilitates optimal heat transfer from the flame to the water, avoiding damage resulting from localized heat loads. Additionally, radiation from soot enhances coal combustion, reducing unburned fuel. Investigations into the flame structure of pulverized coal combustion have been conducted on laboratory-scale burners to attain high thermal efficiency and low emissions from combustion. Significant advancements have been made in understanding pulverized coal flame structure, the progression from polycyclic aromatic hydrocarbons (PAHs) to soot, and eventual oxidation. The pulverized coal flame is formed through intricate interactions among individual pulverized coal particles. Moreover, the combustion of an individual pulverized coal particle has been observed near the burner nozzle of a pulverized coal jet flame[3–6]. Nevertheless, the limited spatial resolution of the camera hinders detailed measurements of the flame structure of a single pulverized coal particle. Understanding the local structure of a pulverized coal flame using a laboratory-scale burner leads to understanding of the flame as a whole. To discuss the local structure of a pulverized coal flame, it is essential to comprehend the combustion behavior of a single pulverized coal particle.

Combustion experiments with single pulverized coal particles offer valuable insights into the factors influencing pulverized coal combustion under various conditions. The ignition of a single pulverized coal particle is a minuscule phenomenon, but through optical measurement, single pulverized coal particles can be observed without disrupting the combustion process. Si et al. constructed a hyperspectral imaging device and observed the combustion behavior of single coal particles[7]. Köser et al. performed first-of-its-kind high-speed planar laser-induced fluorescence(PLIF) measurements of the hydroxyl radical(OH) in the boundary layer of single coal particles[8]. They showed the temporal evolution of the coal particles' reaction zone and the post-combustion zone during combustion. Adeosun et al. performed high-speed backlit imaging with blue LEDs to visualize single particles and compare the emission intensity of coal particles to study their ignition behavior[9]. Wu et al. and Yao et al. used high-speed digital in-line holography (DIH) to visualize particles and volatiles in pulverized coal combustion[10, 11]. Wu et al. visualized typical modes of the volatile flame with respect to the coal particle, including the envelope volatile flame, attached wake flame, detached wake flame, side volatile flame, and combustion of groups of particles[10]. Experiments utilizing OH-PLIF measurement, high-speed backlit imaging, and high-speed DIH have been conducted to understand the ignition behavior, volatile combustion process, and soot formation behavior of single pulverized coal particles. These experiments provided visualization of the formation of envelope flames and wake flames of individual pulverized coal particles. However, the detailed structure of the volatile flame remains unelucidated due to the lack of simultaneous visualization of volatile matter and the flame zone. Simultaneous measurements of laser-induced incandescence, laser-induced scattering, and PAHs-LIF have been utilized to comprehend soot formation in pulverized coal flames[3–6, 12, 13]. These experiments have exhibited the potential to classify the combustion behavior and volatile flame structure of single pulverized coal particles. Visualization of the flame zone and the presence of soot and PAHs is necessary to understand soot formation in single pulverized coal[14, 15]. Although CH_2O-LIF is an effective tool for flame zone visualization, it may interfere with the PAHs-LIF signal, and its effect on pulverized coal flames remains unclear.

Comparing the flame structure of single pulverized coal particles with previous studies of lab-scale burners contributes to a comprehensive understanding of the pulverized coal flame. This study aims to reveal the variety of flame structures a single pulverized coal particle including the soot formation characteristics through the simultaneous imaging of PAHs-PLIF, CH_2O-PLIF, LII, and LIS.

2 Experimental setup and methods

To learn the fundamentals of the volatile flame structure of single pulverized coal particles, a counterflow burner was employed. Figure 1 shows a schematic of the entire device, including the optical system, and a direct image of the counterflow burner [16, 17]. The gas and pulverized coal were supplied under the condition of simulating the transportation of pulverized coal by air. An air-coal (bituminous coal) mixture was supplied from the top port. A mixture of hydrogen and nitrogen was supplied as fuel from the bottom port to form a high-temperature field. As hydrogen was used, soot was formed only from pulverized coal. Table 1 shows the flow conditions for the top and bottom ports. This study investigated the release of volatile matter from pulverized coal particles and the growth of volatile matter to soot by comparing the existing regions of PAHs and soot.

The combustion behavior of single pulverized coal particles was measured by attaching a long working distance microscope (UWZ300F, Union Optical) to an intensified CCD (ICCD) camera (DH334T-25U-03, Andor Technology). This study uses two ICCD cameras for simultaneous laser imaging. The measurement was performed using a camera (ICCD1) installed at 90 °to the laser sheet and a second camera (ICCD2) installed at an angle to the laser sheet. ICCD2 was placed to the left of ICCD1, at an angle of 10 °with respect to ICCD1, and image correction was required. The distortion at the edge of the imaging area was investigated using a scale. The right edge became slightly smaller, and the ratio was 0.3% of the length of the left edge. There was an error of 1 pixel for every 4 mm. The volatile flame formed by a single pulverized coal particle was less than 1 mm, and the error was less than 1 pixel. Therefore, the effect of installing the camera at an angle to the laser sheet can be ignored in this study. The deviation in the scale and position of the imaging area between the cameras was corrected by image processing. ICCD's optical filter and gate timing were appropriately selected for each measurement.

Table 2 shows the detection wavelength and the gate timing of the camera in each laser measurement. The third harmonic (355 nm) of the Nd: YAG laser (Quanta-Ray, Spectra Physics) was used as the excitation light source for the simultaneous measurement of PAHs-PLIF and LII. The second harmonic (532 nm) was used as the excitation light source for the simultaneous measurement of LII and LIS. The PAHs-LIF system eliminates the excitation laser and detects fluorescence within a range of 400 to 700 nm, facilitated by the use of a UV-IR cut filter (UV IR CUT, Roca Universal Design Co., Ltd.) that enhances the detection of fluorescence from PAHs even at low pulse energy levels due to its broad detection wavelength range. This excitation/detection method can measure 3-7 rings of PAHs contained in the volatile matter. This measurement system is capable of quantifying PAHs present in tar during the primary stage of coal pyrolysis, characterized by the presence of 3-7 aromatic rings[18]. The PAHs-LIF signal acquisition was temporally offset by 10 ns from the laser energy peak. The CH_2O-LIF measurement was conducted using the same optical filters and timing parameters utilized for PAHs-LIF, with the exception of a heightened laser pulse power. CH_2O was used as a marker for preheat zone of the volatile flame[15, 19]. For LII measurements, a bandpass filter with a central wavelength of 400 nm and a FWHM of 60 nm, which is shorter than the excitation wavelength, was employed to restrict the acquisition of the PAHs-PLIF fluorescence signal and facilitate the acquisition of the LII signal. The selected detection wavelength of 400 nm has the advantage of improving the signal-to-noise ratio of the LII signal by avoiding the spontaneous light emission of radical chemical species generated during hydrocarbon fuel combustion, such as OH, CH, and C_2 radicals [20]. The gate timing of the LII signal was delayed by 50 ns from the laser pulse peak to mitigate the superposition of the PAHs-LIF signal, which has a relatively fast decay rate, with the LII signal. The delay is shorter than the lifetime of the LII signal ($\sim$1 μ s)[21], and the delay in this study does not bias the LII measurements in favor of large particles[22, 23]. The gate time was set at 20 ns for LIF measurements and 100 ns for LII measurements to eliminate the effect of emission from the luminous flame on the measurement results. For LIS measurements, an ND filter with a transmittance of 5% (MFND-52-5, Sigma Koki) was installed to protect the sensor from damage and prevent saturation of luminosity. The gate timing was set 10 ns ahead of the laser peak for LIS measurements, with the gate time fixed at 10 ns. By setting the gate timing prior to the laser peak, LII and LIF signals were eliminated from LIS measurement.

Background subtraction, noise removal, resolution adjustment, and position adjustment were performed on the image. A 3 $\times$ 3 median filter and a 5 $\times$ 5 Gaussian filter were used to remove noise. The soot formation behavior was visualized by comparing the signal distributions from PAHs and soot.

Table 1 Flow conditions.

		Top port (Oxidizer + coal)*
X_{O2}	X_{N2}	Cross-sectional average flow velocity [cm/s]
21vol%	79vol%	41.1
		Bottom port (Fuel)
X_{H2}	X_{N2}	Cross-sectional average flow velocity [cm/s]
34.5vol%	65.5vol%	50.6

* Coal feeding rate: 6.1 mg/s (ϕ_{coal} = 0.306)

Soot particle size (D_{soot}) and number density (N) are related to signal intensity. LII signal intensity (I_{LII}) is approximately proportional to $N \times D^3_{soot}$, and LIS signal intensity (I_{LIS}) is approximately proportional to $N \times D_{soot}{}^6$ [24, 25]. From these relationships, N was calculated as I^2_{LII}/I_{LIS}, and D_{soot} was calculated as $(I_{LIS}/I_{LII})^{1/3}$. The soot size is nanoscale, and it is difficult to calibrate the measured values. Therefore, this study grasped the qualitative soot distribution calculated from the LII and LIS signal intensities. Figures 2 show the profile of the laser sheet acquired by the beam profiler (L11059, Ophir). The width at which the intensity becomes $1/e^2$, of the maximum value is defined as the thickness of the laser sheet. The laser sheet thickness was 254 μ m at 355 nm and 231 μ m at 532 nm, the height was 20 mm.

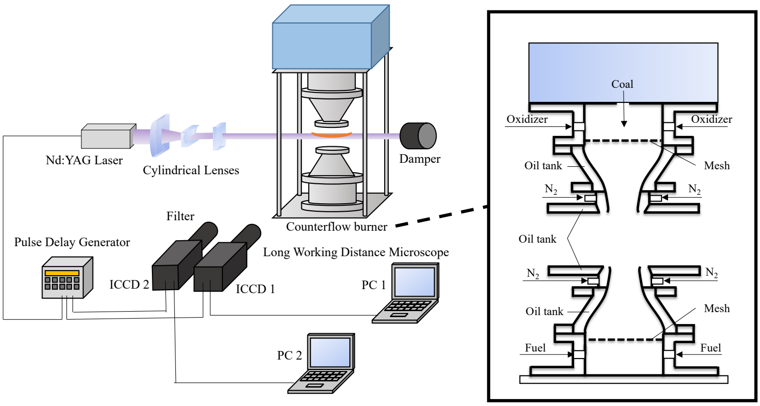

Fig. 1 Schematic diagram of a counterflow burner and measurement setup for laser imaging.

Table 2 Setting of the laser imaging.

	Excitation wavelength	Optical filter	ICCD gate width	ICCD gate delay
PAHs-LIF CH_2O-LIF	355nm	400∼700 nm	20 ns	10 ns
LII	355 nm, 532 nm	370∼430 nm	100 ns	50 ns
LIS	532 nm	ND filter(T = 5%)	10 ns	-10 ns

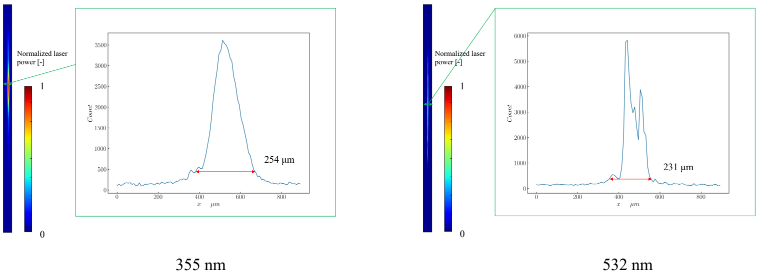

Fig. 2 Laser sheet profile and thickness ($1/e^2$ width)

3 Results and discussion

3.1 Flame structure of volatile flames

PAHs-LIF were conducted at laser pulse energies of 3 mJ and 15 mJ. Through a comparison of the signal distributions, we explored the potential for CH_2O-LIF measurement with the same excitation laser employed in PAHs-LIF. Since emissions within the 400∼700 nm range are detected for the LIF measurement of this study, the potential of crosstalk between the LIF signal, nascent C2 Swan emission, and the LII signal. In the downstream region of the combustion field, soot is present resulting from the combustion of volatile matter without PAHs and the flame zone. The LII signal is detected from this soot, while the LIF signal is not observed. However, careful management of the image intensifier's delay and gate width ensures that the LII signal and C2 Swan emission do not contaminate the LIF signal. The laser pulse was initially set to 3 mJ at a wavelength of 355 nm. Figure 3 displays PAHs-LIF images that capture the typical combustion behavior of single pulverized coal particles. The combustion behavior of these particles is classified into categories (a) through (e) in Figure 3. The signal intensity was normalized to the maximum PAHs-LIF signal intensity. The red arrow indicates the location of the pulverized coal particles, while the green line surrounds the location of the volatile flame. Based on Figure 3, it can be observed that the PAHs-LIF signal exists in a circular shape, with the maximum PAHs-LIF signal near the center of the region. As PAHs are present in the volatile matter, it is presumed that the pulverized coal particles are in the region where the PAHs-LIF signal intensity is highest. Figure 3 (b) reveals the annular PAHs-LIF signal region. The PAHs-LIF signal's minimum intensity is present near this region's center. The inside of the annular PAHs-LIF signal region has a diameter of around 100 μ m. Previous studies conducted using OH-PLIF have demonstrated similar shapes of signal regions[8]. PAHs-LIF signal may be obstructed by the pulverized coal particles because their size is approximately equal to the thickness of the laser sheet. Figure 3 (c) reveals an arc PAHs-LIF signal, likely caused by the non-uniform release of the volatile matter. Figure 3 (d) depicts the behavior of pulverized coal particle which exit the volatile flame. The larger area illustrates the volatile flame, while the smaller area represents the pulverized coal particle. Pulverized coal particles may have been carried away from the volatile flame due to the non-uniform combustion of volatiles, resulting in their escape. It is apparent that the release of volatile matter from the pulverized coal persists even after the pulverized coal particles have escaped the volatile flame. Figure 3 (e) displays the streaky PAHs-LIF signal region. Previous studies utilizing high-speed imaging and DIH measurement also demonstrated the behavior of the formed soot to aggregate in a streaky region[11, 16]. The signal distribution of LII demonstrated an equivalent distribution pattern with that of PAHs-LIF.

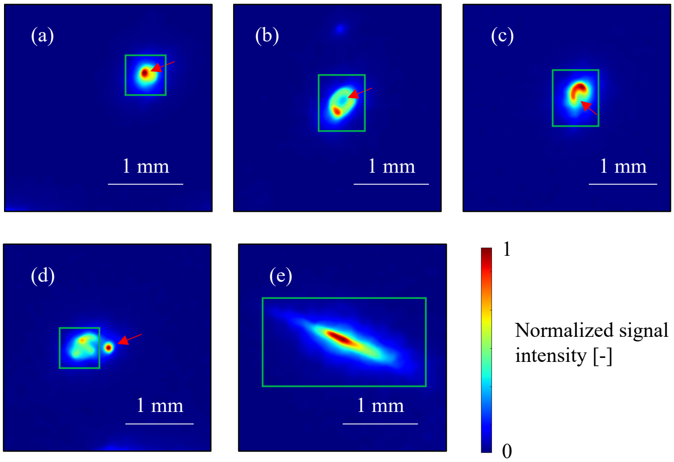

Fig. 3 Typical combustion behavior of single coal particle measured by PAHs-LIF. (a) circular region (b) annular region (c) arc region (d) two separated regions (e) line shaped region

To examine the volatile flame structure, the region containing PAHs and soot signals was analyzed. Figure 4 illustrates the distribution of PAHs-LIF and LII signals, along with an overlay of two typical combustion behaviors of pulverized coal. The flame structure of pulverized coal particles inside the volatile flame was investigated. The overlaid image was converted into binary format before normalization of each signal using the maximum value. A threshold value of 10 times the background noise level was utilized to detect only the area where the signal is present. Figure 4 (a) demonstrates the signal distribution when pulverized coal particles are present in the volatile flame. The positions of the maximum values of each signal are identical. The overlaid image reveals the presence of the PAHs-LIF signal inside the LII signal, which indicates the diffusion flame structure of the volatile flame. Figure 4 (b) shows the signal distribution when pulverized coal particles are present outside of the volatile flame. The small signal region in the PAHs-LIF image contains pulverized coal particles, whereas the large signal region corresponds to volatile flames. The volatile flame possesses a diffusion flame structure similar to that shown in Fig.4 (a). However, the region with weak LII signals extends around the pulverized coal particle surrounded by the green line in Fig.3 (b). This result demonstrates that the separation of the pulverized coal particles from the volatile flame hindered the increase in volatile concentration inside the volatile flame and reduced the formation of soot.

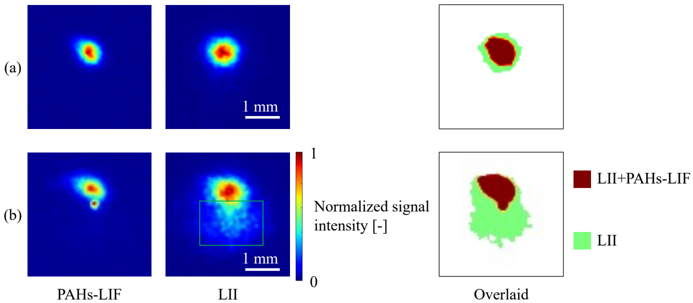

Fig. 4 Combustion behavior of single coal particle by simultaneous imaging of PAHs-LIF and LII. (a) Envelope flame (b) Coal particles escaped from volatile flame

Subsequently, laser imaging was conducted with an elevated laser pulse energy of 15 mJ, while CH_2O-LIF measurements were performed simultaneously. Figure 5 exhibits an image of the PAHs-LIF measurement. Figure 5 (a) portrays the PAHs-LIF measurement image, while (b) shows the labeled image after binarizing image (a). Figure 5 illustrates six areas with PAHs-LIF signals, and the signal distribution can be classified into two types. Distribution (1) has a maximum value in the center of the region, and distributions (2) to (6) have a maximum value near the edge of the region. The PAHs-LIF measurement did not show the distributions (2) to (6) under the condition of 3 mJ laser pulse energy. Therefore, PAHs-LIF signals and other signals were detected under the condition of 15 mJ laser pulse energy. Signal intensity histograms for each area were compared. Figure 6 depicts signal intensity histograms for the six areas labeled in Fig. 5 (b). Only distribution (1) two peak signals, whereas the others have one peak signal. Therefore, the peak of the higher signal intensity in the distribution (1) is presumed to be the PAHs-LIF signal located in the center of the region. The lower signal intensity peak of distribution (1), and the signal intensities of distributions (2) to (6) are lower than the PAHs-LIF signal. Consequently, these signals may differ from PAHs-LIF signals. This signal has a maximum at the edge of the area, with an excitation wavelength of 355 nm and a detection length of 400-700 nm. Therefore, this LIF measurement is speculated to detect the CH_2O-LIF signal. The signal peak at the edge of the region indicated the flame front of the volatile flame. CH_2O-PAHs-LIF/LII simultaneous imaging visualized PAHs, soot, and the flame front in volatile flames. Figure 7 displays three typical flame structures. Figure 7 (a) shows the envelope flame during volatile matter release, (b) shows the enveloping flame after volatiles release, and (c) exhibits pulverized coal particles escaping the volatile flame. The left image displays the original image of the CH_2O-PAHs-LIF measurement, the middle image displays the original image of the LII measurement, and the right image shows Overlay the binarized image. Figure 7 (a)(b) illustrated the existence of LII signal area inside the CH_2O-PAHs-LIF signal area when the perimeter flame was formed.

These results indicate a diffusion flame structure of the volatile flame. Figure 7 (b) illustrates that the volatile flame has a diffusion flame structure and forms a biased flame. The lopsided volatile flame may be the effect of asymmetric volatile release from pulverized coal particles. The effective diameter of CH_2O-PAHs-LIF measurements was compared with that of LII measurements. Figure 8 displays the original image of CH_2O-PAHs-LIF measurement, the original image of LII measurement, and the binarized image. Each area is labeled with a number from 1 to 5, and the numbers in parentheses indicate the effective diameter ratio of the CH_2O-PAHs-LIF signal to the effective diameter of the LII signal (D_{LIF}/D_{LII}). The results of the measurement demonstrated D_{LIF}/D_{LII} values within the range of 2-3. The LII signal identified in Fig. 8(4) represents an independent area for each volatile flame, while the CH_2O-PAHs-LIF signal shows two regions combined into a single region. These results indicate that the soot formation region operates independently, whereas the flame front is connected between two pulverized coal particles. Moreover, the results suggest that LII measurements underestimate the diameter of volatile flames.

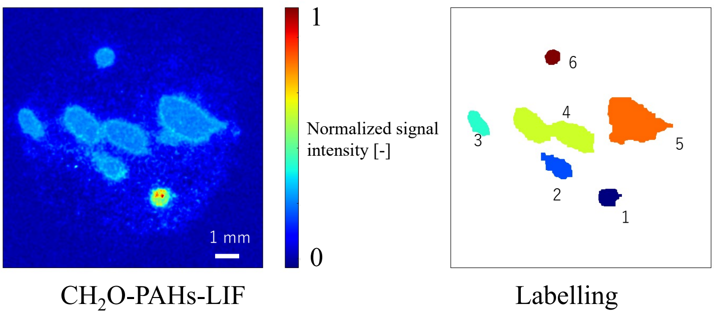

Fig. 5 Original and labeled images of CH_2O-PAHs-LIF signal.

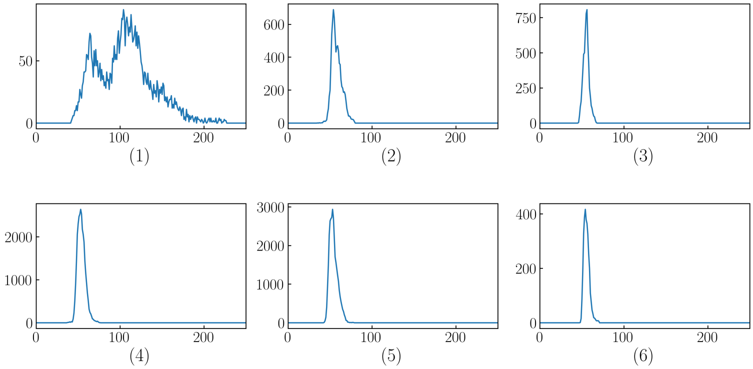

Fig. 6 Histogram of signal intensity in each region.

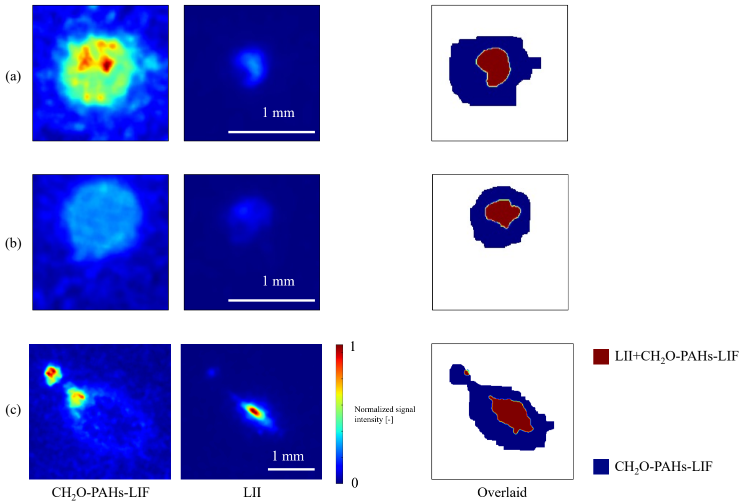

Fig. 7 Typical combustion behavior measured by simultaneous imaging of CH_2O-PAHs-LIF and LII.

3.2 Soot Distribution in Volatile Flame

Figure 9 depicts the distribution of signals (a) LII signal (in blue) and the LIS signal (in red), soot particle size distribution (b), and soot number density distribution (c) during volatile combustion. The investigation of soot number density and size was carried out qualitatively due to the challenges involved in calibrating soot measurements. The qualitative soot particle size distribution was evaluated using the formula $(I_{LIS}/I_{LII})^{1/3}$, and the soot number's density distribution was computed as I^2_{LII}/I_{LIS} using the LII signal intensity (I_{LII}) and the LIS signal intensity (I_{LIS}). Figure 9 demonstrates that the soot number density decreases from the inner part to the area's outer periphery, and the soot particles' size tends to increase. The green arrow indicates the location of the pulverized coal particle determined from the LIS signal. This

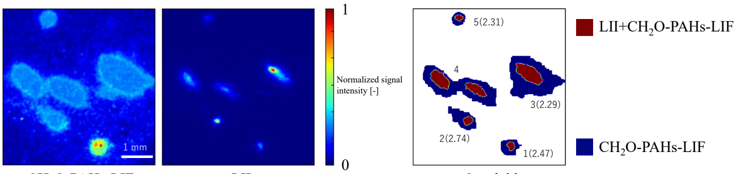

Fig. 8 Comparison of flame diameters measured by simultaneous imaging of CH_2O-PAHs-LIF and LII.

implies that the soot grows in the volatile flame. Furthermore, Figures 9 (i), (ii), and (iii) exhibit that the soot distribution has a few local signal peaks. This tendency was observed when the signal area was small. The generation of soot may have been non-uniform due to the low release of volatile matter from smaller coal particles. Figure 9 (iv) illustrates that solely the LIS signal was discerned from the coal particles, which implies that the laser pulse energy was accurately regulated and the coal particles were not heated to redness by the laser pulse. In Figure 9 (v), it can be seen that soot formation continues even from the particles that have escaped from the volatile flame, and soot is present near the pulverized coal particles. In the case of Fig. 9 (v), the LIS signal from the pulverized coal particles is superimposed on the LIS signal from the soot, and the soot particle size is overestimated. Hence, it is necessary to consider the scattered light from pulverized coal particles in soot measurement using LIS/LII simultaneous measurement. Figure 9(vi) shows streaky signal distribution. The volatile flame would have been deformed by the flow near the stagnation plane. When the pulverized coal particle size is larger than the laser sheet thickness, the pulverized coal intercepts the signal from the volatile flame. The laser sheet thickness is larger than the median diameter of the pulverized coal used. Therefore, the frequency of this phenomenon may have been low. Finally, it is observed that the soot number density in Fig. 9 (vi) was small, and the size of the signal area was large. The soot would have grown and agglomerated, resulting in a reduced amount of soot. Therefore, (vi) would be the combustion behavior in the late stage of volatile combustion. Similar combustion behavior was also observed in the latter stage of the volatile combustion process by high-speed imaging and Digital Inline Holography[11].

4 Conclusion

The aim of this study was to understand the soot formation process in bituminous coal by constructing a simultaneous laser imaging system for CH_2O-LIF, PAHs-LIF, LII, and LIS measurements during the volatile combustion of a single pulverized coal particle. The variety of flame structures a single pulverized coal particle including the soot formation characteristics was investigated by comparing the areas where each signal exists by using simultaneous laser imaging. The results indicated the feasibility of CH_2O-LIF, PAHs-LIF, LII, and LIS measurements for a single pulverized coal particle. By appropriately

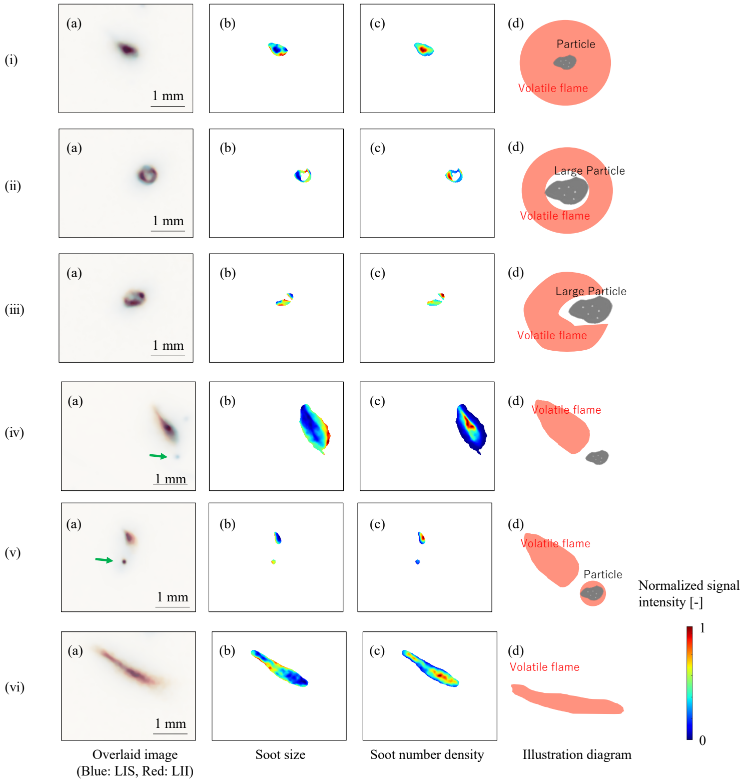

Fig. 9 Size and number density distribution of soot in volatile flames measured by simultaneous imaging LII and LIS.

adjusting the laser pulse energy, it was possible to measure CH_2O-PAHs-LIF for single pulverized coal combustion and to prevent the pulverized coal particles from reaching the temperature at which they emit visible light. However, the determination of the volatile flame diameter from the LII signal resulted in underestimation, while determining the flame diameter from the CH_2O-LIF signal was effective in grasping the volatile flame. The calculated effective flame diameter from the CH_2O-LIF signal was larger than the effective flame diameter calculated from the LII signal. To understand the local flame structure of pulverized coal, it is crucial to investigate the combustion behavior of a single pulverized coal particle. This results will enhance our comprehension of local flame structure and support the development of pulverized coal combustion models. The present measurement system will be used to analyze the combustion of clusters of pulverized coal, further enhancing our understanding of pulverized coal flames.

Acknowledgments. We would like to thank Editage (www.editage.com) for English language editing.

Declarations

The authors declare no conflicts of interest associated with this manuscript.

References

[1] Morris, J., Hone, D., Haigh, M., Sokolov, A., Paltsev, S.: Future energy: in search of a scenario reflecting current and future pressures and trends. Environmental Economics and Policy Studies **25**(1), 31–61 (2022). https://doi.org/10.1007/s10018-021-00339-1

[2] Blokh, A.G.: Heat transfer in steam boiler furnaces (1987)

[3] Hashimoto, N., Hayashi, J., Nakatsuka, N., Tainaka, K., Umemoto, S., Tsuji, H., Akamatsu, F., Watanabe, H., Makino, H.: Primary soot particle distributions in a combustion field of 4 kw pulverized coal jet burner measured by time resolved laser induced incandescence (tire-lii). Journal of Thermal Science and Technology **11**(3), 0049–0049 (2016). https://doi.org/10.1299/jtst.2016jtst0049

[4] Hashimoto, N., Hayashi, J.: Coal particle devolatilization and soot formation in pulverized coal combustion fields. KONA Powder and Particle Journal **38**, 168–188 (2021). https://doi.org/10.14356/kona.2021003

[5] Hayashi, J., Hashimoto, N., Nakatsuka, N., Tainaka, K., Tsuji, H., Tanno, K., Watanabe, H., Makino, H., Akamatsu, F.: Simultaneous imaging of mie scattering, pahs laser induced fluorescence and soot laser induced incandescence to a lab-scale turbulent jet pulverized coal flame. Proceedings of the Combustion Institute **37**(3), 3045–3052 (2019). https://doi.org/10.1016/j.proci.2018.09.028

[6] Hayashi, J., Tainaka, K., Fukada, T., Muto, M., Kawanabe, H., Kurose, R.: Soot formation characteristics in a pulverized coal flame formed in a swirling flow. Advanced Powder Technology **31**(9), 3921–3927 (2020). https://doi.org/10.1016/j.apt.2020.07.028

[7] Si, M., Cheng, Q., Yuan, L., Luo, Z., Yan, W., Zhou, H.: Study on the combustion behavior and soot formation of single coal particle using hyperspectral imaging technique. Combustion and Flame **233**, 111568 (2021). https://doi.org/10.1016/j.combustflame.2021.111568

[8] Köser, J., Becker, L., Vorobiev, N., Schiemann, M., Scherer, V., Böhm, B., Dreizler, A.: Characterization of single coal particle combustion within oxygen-enriched environments using high-speed oh-plif. Applied Physics B **121**, 459–464 (2015)

[9] Adeosun, A., Xiao, Z., Gopan, A., Yang, Z., Wang, X., Li, T., Yao, Q.,

Axelbaum, R.L.: Pulverized coal particle ignition in a combustion environment with a reducing-to-oxidizing transition. Journal of the Energy Institute **92**(3), 693–703 (2019). https://doi.org/10.1016/j.joei.2018.03.003

[10] Wu, Y., Yao, L., Wu, X., Chen, J., GrÃ©han, G., Cen, K.: 3d imaging of individual burning char and volatile plume in a pulverized coal flame with digital inline holography. Fuel **206**, 429–436 (2017). https://doi.org/10.1016/j.fuel.2017.06.031

[11] Yao, L., Wu, C., Wu, Y., Chen, L., Chen, J., Wu, X., Cen, K.: Investigating particle and volatile evolution during pulverized coal combustion using high-speed digital in-line holography. Proceedings of the Combustion Institute **37**(3), 2911–2918 (2019). https://doi.org/10.1016/j.proci.2018.06.179

[12] Balusamy, S., Kamal, M.M., Lowe, S.M., Tian, B., Gao, Y., Hochgreb, S.: Laser diagnostics of pulverized coal combustion in o 2/n 2 and o 2/co 2 conditions: velocity and scalar field measurements. Experiments in Fluids **56**, 1–16 (2015)

[13] Hwang, S.m., Kurose, R., Akamatsu, F., Tsuji, H., Makino, H., Katsuki, M.: Application of optical diagnostics techniques to a laboratory-scale turbulent pulverized coal flame. Energy & fuels **19**(2), 382–392 (2005)

[14] Wang, Z., Stamatoglou, P., Li, Z., Aldén, M., Richter, M.: Ultra-high-speed plif imaging for simultaneous visualization of multiple species in turbulent flames. Opt. Express **25**(24), 30214–30228 (2017). https://doi.org/10.1364/OE.25.030214

[15] Jiang, N., Hsu, P.S., Grib, S.W., Roy, S.: Simultaneous high-speed imaging of temperature, heat-release rate, and multi-species concentrations in turbulent jet flames. Opt. Express **27**(12), 17017–17026 (2019). https://doi.org/10.1364/OE.27.017017

[16] Sawada, S., Okada, D., Nakatsuka, N., Tainaka, K., Hori, T., Hayashi, J., Akamatsu, F.: Time-series temperature measurement during combustion of volatile matter and coal char of a single pulverized coal particle via magnified two-color pyrometry with blue backlit imaging. Energy & Fuels **34**(10), 12918–12925 (2020) https://arxiv.org/abs/https://doi.org/10.1021/acs.energyfuels.0c01246. https://doi.org/10.1021/acs.energyfuels.0c01246

[17] Sawada, S., Okada, D., Nakatsuka, N., Tainaka, K., Hori, T., Hayashi, J., Akamatsu, F.: Effects of ambient temperature on the combustion processes of single pulverized coal particle. Journal of Thermal Science and Technology **16**(1), 0011–0011 (2021). https://doi.org/10.1299/jtst.

2021jtst0011

[18] Bejaoui, S., Mercier, X., Desgroux, P., Therssen, E.: Laser induced fluorescence spectroscopy of aromatic species produced in atmospheric sooting flames using uv and visible excitation wavelengths. Combustion and Flame **161**(10), 2479–2491 (2014). https://doi.org/10.1016/j.combustflame.2014.03.014

[19] Wang, Z., Stamatoglou, P., Zhou, B., AldÃ©n, M., Bai, X.-S., Richter, M.: Investigation of oh and ch2o distributions at ultra-high repetition rates by planar laser induced fluorescence imaging in highly turbulent jet flames. Fuel **234**, 1528–1540 (2018). https://doi.org/10.1016/j.fuel.2018.07.012

[20] Schulz, C., Kock, B.F., Hofmann, M., Michelsen, H., Will, S., Bougie, B., Suntz, R., Smallwood, G.: Laser-induced incandescence: recent trends and current questions. Applied Physics B **83**, 333–354 (2006)

[21] Michelsen, H.A., Schulz, C., Smallwood, G.J., Will, S.: Laser-induced incandescence: Particulate diagnostics for combustion, atmospheric, and industrial applications. Progress in Energy and Combustion Science **51**, 2–48 (2015). https://doi.org/10.1016/j.pecs.2015.07.001

[22] Oh, K.C., Shin, H.D.: The effect of oxygen and carbon dioxide concentration on soot formation in non-premixed flames. Fuel **85**(5), 615–624 (2006). https://doi.org/10.1016/j.fuel.2005.08.018

[23] Hayashi, J., Watanabe, H., Kurose, R., Akamatsu, F.: Effects of fuel droplet size on soot formation in spray flames formed in a laminar counterflow. Combustion and Flame **158**(12), 2559–2568 (2011). https://doi.org/10.1016/j.combustflame.2011.05.015

[24] Lee, K.H., Chung, J.W., Kim, B.S., Kim, S.K.: Investigation of soot formation in a di diesel engine by using laser induced scattering and laser induced incandescence. KSME international journal **18**, 1169–1176 (2004)

[25] Lee, K., Han, Y., Lee, W., Chung, J., Lee, C.: Quantitative measurements of soot particles in a laminar diffusion flame using a lii/lis technique. Measurement Science and Technology **16**(2), 519 (2005). https://doi.org/10.1088/0957-0233/16/2/026